Journal of Alloys and Compounds 523 (2012) 108–113

Contents lists available at SciVerse ScienceDirect

Journal of Alloys and Compounds

journal homepage: www.elsevier.com/locate/jallcom

On the effect of thermal treatment and hydrogen vibrational dynamics in sodium alanates: An inelastic neutron scattering study

A. Albinati[a,*], D. Colognesi[b], P.A. Georgiev[a], C.M. Jensen[c], A.J. Ramirez-Cuesta[d]

[a] Dipartimento di Chimica Strutturale e Stereochimica Inorganica, Università degli Studi di Milano, via G. Venezian 21, 20133 Milan, Italy
[b] Consiglio Nazionale delle Ricerche, Istituto di Sistemi Complessi, via Madonna del Piano 10, 50019 Sesto Fiorentino (FI), Italy
[c] Department of Chemistry, University of Hawaii, Honolulu, HI 96822, USA
[d] ISIS facility, Rutherford Appleton Laboratory, Chilton, Didcot OX11 0QX, UK

ARTICLE INFO

Article history:
Received 14 October 2011
Received in revised form 15 January 2012
Accepted 16 January 2012
Available online 26 January 2012

Keywords:
Metal hydrides
Neutron scattering
Spectroscopy
DFT

ABSTRACT

We have measured inelastic neutron scattering (INS) spectra from Ti-doped polycrystalline alanates ($NaAlH_4$ and Na_3AlH_6), at low temperature, in the energy transfer range 3–500 meV, both for thermally treated and untreated samples. From the spectral range corresponding to the fundamental vibrational bands of these aluminohydrides, accurate one-phonon spectra and hydrogen-projected densities of phonon states have been extracted and analyzed using *ab initio* lattice dynamics calculations. Satisfactory agreement has been found for the untreated samples. In the case of thermally treated samples, due to thermal decomposition, different ionic species are present and the sample composition could be quantitatively evaluated. No evidence for the existence of intermediate species such as AlH_3 or AlH_5^{2-} has been found.

1. Introduction

The possibility of using hydrogen as an environmentally friendly and efficient fuel is very actively investigated [1,2], but an efficient way of storing hydrogen is still an unsolved problem. In fact, applications such as on-board storage for automotive uses or hydrogen fuelled portable electronics will require new materials that can store large amounts of hydrogen (more than 5 wt.%, H_2) at ambient, or close to ambient, temperature and relatively low pressures with small volume, low weight, and fast kinetics for charging/discharging. Metal hydrides [3] carbon-based nanomaterials (such as metal-doped carbon nanotubes) and MOFs have been studied [4], but there are still many problems associated with their practical implementation, including cost, low specific uptake, unfavorable thermodynamics and/or kinetics etc. Binary ionic hydrides of the elements of groups 1, 2 and 13 such as $M(EH_4)_x$, (M = Li, Na, K, Mg or Ca, and E = Al or B) have been studied as promising materials. In particular, sodium alanates (*i.e.* $NaAlH_4$ and Na_3AlH_6) have attracted a great deal of interest since Bogdanović and Schwickardi [5] have shown that the hydrogenation reaction can be kinetically enhanced and rendered reversible, under mild conditions, after doping with transition metal halides such as MX_3 (M = Ti, Zr, Co, Ni, or Fe; X = F, Cl, or I). The relevant reversible reactions involved in the process are:

$$3NaAlH_4 \leftrightarrows Na_3AlH_6 + 2Al + 3H_2(3.7\,wt.\%) \quad (I)$$

$$Na_3AlH_6 \leftrightarrows 3NaH + Al + 3/2H_2(1.8\,wt.\%) \quad (II)$$

These reactions occur at moderate pressures ($p < 100$ bar) and temperatures ($T < 438$ K), so the doped $NaAlH_4$-plus-Na_3AlH_6 system exhibits characteristics not too far from those required for practical applications. However, much work is still necessary to improve the storage properties of the alanates, and to this aim a detailed understanding of the H_2 absorption/desorption process is crucial. A microscopic mechanism of the catalytic processes in Ti-doped $NaAlH_4$ has been recently suggested [6–8], but not yet experimentally validated. Moreover, recent "anelastic relaxation" measurements [9] have shown that after thermal activation (at temperatures in the range 370–436 K) a new species appears in Ti-doped sodium alanates (and to a very much less extent also in those undoped). This species gives rise to a thermally activated relaxation at $T \approx 70$ K and $\nu = 1$ kHz, with an activation energy of $E = 0.126$ eV, and a pre-exponential factor of $\tau = 7 \times 10^{-14}$ s, typical values for a point-defect relaxation. This reactive species shows a fast dynamics and, according to the deuterium isotopic effect found, involves hydrogen. These observations are consistent with the formation, upon thermal treatment, of a distorted octahedral defect of type AlH_x^{n-} ($x < 6$), causing a local vacancy dynamics. The formation of such defects appears to be catalyzed by the presence of the Ti dopant [9].

* Corresponding author.
E-mail address: Alberto.Albinati@unimi.it (A. Albinati).

0925-8388/$ – see front matter © 2012 Elsevier B.V. All rights reserved.
doi:10.1016/j.jallcom.2012.01.094

Table 1
Sample description, including doping amount, thermal treatment temperature, experimental temperature T, Integrated Proton Current (IPC), and mass. One hour of counting time corresponds approximately to 150 μA h IPC.

#	Sample	Ti doping (mol.%)	Thermal treat. (K)	T (K)	IPC (μA h)	Mass (mg)
1	$NaAlH_4$	4	–	16 (2)	543.7	762
2	$NaAlH_4$	4	435	16 (2)	453.1	698
3	Na_3AlH_6	4	–	16 (2)	818.8	725
4	Na_3AlH_6	4	435	16 (2)	1146.3	811

The present work aims at extending the microscopic investigation of the effect of the thermal treatment on the proton dynamics in doped $NaAlH_4$ and Na_3AlH_6, (before and after thermal treatment) by using high-resolution inelastic neutron scattering (INS). Compared to Raman and infrared spectroscopy, INS allows, more easily and reliably, the separation of the various contributions stemming from different atoms. Moreover, neutron vibrational mode intensities can be accurately reproduced by lattice dynamics simulations [10].

Previously, inelastic neutron scattering studies have been performed on $NaAlH_4$ (pure and 2% Ti-doped) and on Na_3AlH_6 [11], with an energy resolution of 2–4.5% in the energy transfer range (50–250) meV; an INS study on $NaAlH_4$ was also carried out by Fu et al. [12], using a larger energy transfer range (3 meV < E < 500 meV) and greater energy resolution (1.5–3%). While the former work has been aimed at providing some microscopic understanding of the role of the Ti-additive in $NaAlH_4$ and its specific occurrence in the material, the latter work has been mainly focused on the spectral modifications of doped samples after several H_2 charging/discharging cycles of $NaAlH_4$ only. In contrast, our work is focused on the search for spectral evidences for the H-containing extra-species or defect structures responsible for the observations by "anelastic relaxation" experiments [9] after thermal treatment of both $NaAlH_4$ and Na_3AlH_6. Additionally, some essential improvements of the instrumentation used regarding resolution, background levels and sensitivity have been achieved since the previous work [12].

2. Experiment description

The neutron scattering measurements were carried out on the TOSCA-II inelastic spectrometer at the ISIS neutron source. TOSCA-II is a crystal-analyzer inverse-geometry spectrometer [13] spanning a broad energy range transfers ($E = E_0 - E_1$, 3 meV < E < 500 meV), with an energy resolution $\Delta E/E_0 \cong 1.5$–3%.

Special care was taken to prevent possible wetting and decomposition of the alanates, during the sample loading, in a flat Al scattering-cell that was performed in a glove box under He atmosphere. Four samples were used for the data collections:

(1) $NaAlH_4$, recrystallized from tetrahydrofuran, and doped with 4 mol.% TiF_3 by ball milling (30 min at 350 rpm) [14].
(2) $NaAlH_4$, recrystallized from tetrahydrofuran, doped with 4 mol.% TiF_3 by ball milling (30 min at 350 rpm), and thermally treated (1 h at T = 435 K).
(3) Na_3AlH_6, produced and purified via the standard Huot et al. method [15], and doped with 4 mol.% TiF_3 by ball milling (30 min at 350 rpm).
(4) Na_3AlH_6, produced and purified via the standard Huot et al. method [15], doped with 4 mol.% TiF_3 by ball milling (30 min at 350 rpm), and thermally treated (1 h at T = 435 K).

The most important experimental details are given in Table 1; further details on the synthesis, purification and treatment can be found in Ref. [14]; the phase purity of all untreated samples was checked by X-ray powder diffraction using part of each sample batch. Before the neutron data collection, the empty cell was cooled down to the temperature of the experiment: (16 ± 2 K). The INS spectra of the four samples were then measured in the same conditions. The experimental time-of-flight spectra were transformed into energy transfer data by using the standard TOSCA-II data reduction routines. Further details are given in Appendix A.

The resulting INS spectra, proportional to $S(Q,E)$, are reported in Fig. 1.

3. Computational details

Periodic density functional theory calculations were carried out using a plane wave basis-set and pseudopotentials as implemented in the CASTEP code [16–18] The PBE [19] version of the localized density approximation within DFT was used in conjunction with optimized norm-conserving pseudopotentials. The Brillouin zone sampling for the electronic calculations used a 3 × 3 × 2 grid of k-points generated using the Monkhorst–Pack method. A full geometry optimization (with a plane-wave cut-off energy of 770 eV) of the internal atomic co-ordinates was performed to reduce the residual atomic forces to less than 1.5 meV/Å. This procedure converged to the following lattice cell parameters: a = 5.038 Å, c = 11.300 Å for $NaAlH_4$ and a = 5.413 Å, b = 5.546 Å, c = 7.765 Å, β = 89.87° for Na_3AlH_6. These values are in agreement with those obtained by powder diffraction [20] for tetragonal $NaAlH_4$ (a = 5.02508(6) Å, c = 11.3571(2) Å) and for monoclinic Na_3AlH_6 (a = 5.4145(3) Å, b = 5.5402(3) Å, c = 7.7620(4) Å, β = 89.871(4)°).

Phonon modes were calculated using density functional perturbation-theory [16,21] on a 5 × 5 × 3 grid to calculate the dynamical matrix; the Brillouin zone was sampled on a 9 × 9 × 6 grid, using the interpolation algorithm included in CASTEP to obtain a smooth density of phonon states and calculated spectra as described in [10]. The INS spectrum was generated using the program ACLIMAX [22]. Calculations were performed on the complete unit cell using the experimentally determined structural data as input [20]. The corresponding calculated INS spectra are shown together with their experimental counterparts in Fig. 2. The excellent agreement between theory and experiment further confirms the phase purity of the untreated samples.

4. Discussion

The neutron spectra from Ti-doped $NaAlH_4$ and Na_3AlH_6 (see Fig. 1, spectra #1 and #3) may be compared with the results reported in the energy transfer range 35 meV < E < 250 meV in Ref. [11]. Despite an evident similarity in the band positions and intensities, some care is needed in comparing the spectra, since the two

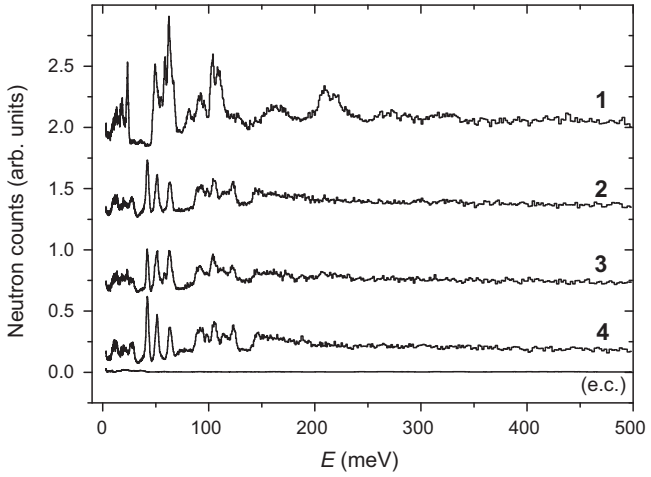

Fig. 1. Examples of raw neutron spectra from samples #1, #2, #3 and #4 as from Table 1 plus the empty cell (e.c.), all recorded in backscattering at T = 16 K. Spectra have been vertically shifted.

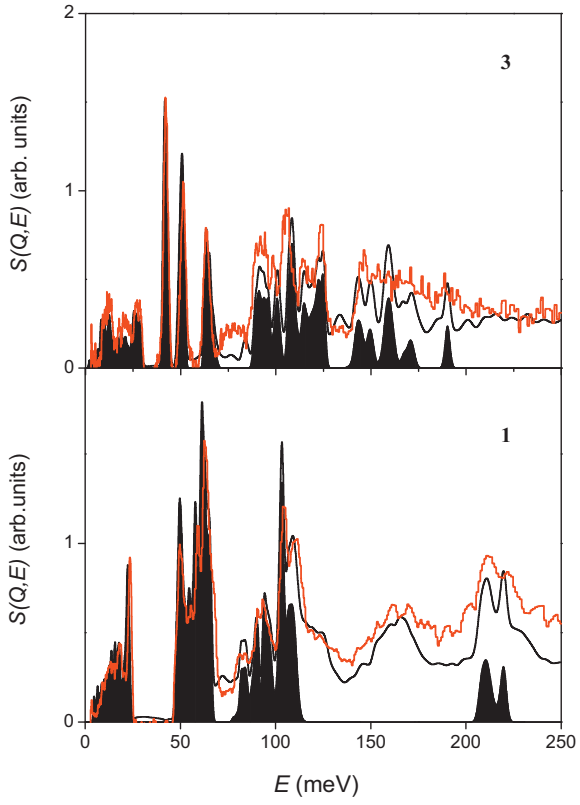

Fig. 2. Calculated (black lines) and experimental (red lines) INS spectra of untreated $NaAlH_4$ – #1 and Na_3AlH_6 – #3. For both compounds, shaded peaks represent the fundamental transitions broadened by dispersion effects and instrumental resolution. (For interpretation of the references to color in this figure legend, the reader is referred to the web version of this article.)

spectrometers used differ both in energy resolution and instrumental geometries. TOSCA has approximately 3 to 4 times better energy resolution than that in Ref. [11] (FANS spectrometer [23]) and, moreover, to each energy transfer point on the TOSCA trajectory corresponds just one exact value for the momentum transfer modulus, Q, which on FANS is averaged over a relatively large scattering angle range. This makes the measured intensities to appear slightly different in the various parts of the spectra accessed by the two instruments. Thus, using these advantages of TOSCA and the output of our DFT calculations, focusing on the H-dynamics, we have been able to identify all of the observed vibrational features for both $NaAlH_4$ and $NaAl_3H_6$.

Four main bands due to proton vibration modes dominate the spectrum of the untreated $NaAlH_4$, Fig. 2 (see also Fig. A4 in Appendix A):

a) lattice collective motions (Na^+ and AlH_4^- sublattices vibrating against each other, transverse and longitudinal vibrations) with the most intense feature centered at 24 meV;
b) AlH_4^- rigid body librations in the region 43–69 meV;
c) Al–H bending and H–Al–H scissoring modes between 74 and 116 meV;
d) Al–H stretching vibrations with maxima at ca. 217 and 225 meV for the symmetric and antisymmetric modes, respectively.

The spectrum of the untreated Na_3AlH_6 sample shown in Fig. 2 (panel 3, see also Fig. A4 in Appendix A) is similar to that of the tetra-hydride: the major difference being the absence of clearly resolved Al–H stretching vibrations. Thus, the assignment of the features seen in the spectrum of the Na_3AlH_6 sample is similar to

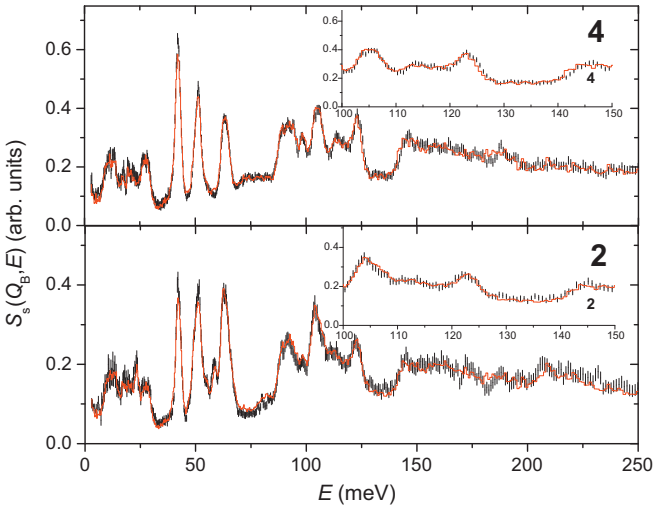

Fig. 3. Generalized self inelastic structure factor from the Ti-doped thermally treated $NaAlH_4$ and Na_3AlH_6 samples (**#2** and **#4**, cf. Table 1), recorded in backscattering at $T = 16$ K (error bars). In addition their best fits using a linear combination of thermally untreated data (namely #3 and #1 and NaH spectrum [24]) have been added as full lines.

that of the tetra-hydride analogue. The lattice collective modes are again observed in the region 6.2–27.8 meV. In contrast to the tetra-hydride, the librations around the three principal axes of the AlH_6^{3-} moiety are well separated at 42, 51, and 64 meV. The Al–H bend and H–Al–H scissoring modes appear between 82 and 120 meV, followed by a rather wide spread of Al–H stretch bands between 140 and 195 meV. The highest energy feature in the spectrum, found at about 195 meV, originates from the AlH_6^{3-} ion breathing mode (symmetric Al–H stretches).

As far as the thermally activated $NaAlH_4$ and Na_3AlH_6 samples are concerned, in Fig. 3 we report their fits showing how the $\Sigma_s(Q,E)$ (see also Appendix A) spectra from samples 2 and 4 can be quite satisfactorily reconstructed by a simple linear combination of their thermally untreated components: Na_3AlH_6 plus $NaAlH_4$ or NaH [24] ($\chi^2 = 0.61$ and 0.62, respectively), leaving no unaccounted vibrational features. Thus, under the conditions of our experiments, after our thermal treatment we have found no evidence for the recently discovered by ^{27}Al NMR [25] highly defective AlH_5^{2-}species. However, these may exist only locally, as an out-of-equilibrium short-lived species near defects created by Ti atoms, for instance. This would certainly render the observation and characterization of such structures very difficult. We note that in the region around 130 meV, both the tetra- and hexa-hydrides spectra are virtually featureless and therefore we might expect quite high sensitivity of the method towards extra species such as AlH_5^{2-} containing large H-molar fraction (of the order of 1–2 wt.% for the used samples).

5. Conclusions

We have collected high resolution incoherent inelastic neutron scattering data from polycrystalline Ti-doped $NaAlH_4$ and Na_3AlH_6 (both thermally treated and untreated), and carried out *ab initio* lattice dynamics calculations to interpret the vibrational spectra. The remarkable differences between the thermally treated and the untreated $NaAlH_4$ and Na_3AlH_6 samples can be explained by the transformations outlined in Eqs. (I) and (II) (cf. Table 1).

From the spectral region corresponding to the fundamental vibrational bands of both (thermally untreated) alanates (3 meV < E < 250 meV), we were able to self-consistently estimate

the respective multiphonon terms and to extract accurate and well-resolved one-phonon spectra and hydrogen-projected densities of phonon states.

The experimental data were compared to the results of *ab initio* lattice dynamics calculations. The overall agreement is quite satisfactory. A further comparison was set up between the experimental hydrogen-projected densities of phonon states and frequencies, simulated through *ab initio* lattice dynamics which also included dispersion effects. These frequency values give a clear physical interpretation to the main neutron spectral bands, and, in some cases, even to few intra-band features. These analyses, however, did not reveal the presence of any other stoichiometric or non-stoichiometric species other than the ones given in Eqs. (I) and (II), *i.e.* $NaAlH_4$, Na_3AlH_6, and NaH. Thus, we do not find any evidence of the formation of the thermally activated species found in Ti-doped alanates by "anelastic relaxation" spectroscopy [9] even though the mean activation energy of this process at $E_a \cong 126$ meV is well in the instrumental spectral energy range. This observation can be explained by the different sensitivity of the two techniques as the "anelastic relaxation" spectroscopy is a much more sensitive technique which can detect intermediates that are only present in catalytic amount, and thus our results indirectly support the "defect-catalyzed" mechanism of activation of Ti-doped alanates. Similarly, we cannot confirm the presence in the activated samples of the recently suggested AlH_3^{2-} defects which are expected to lead to the formation of AlH_5^{2-} anions whose vibrational features are predicted in the energy region between Al–H bending stretching modes of the AlH_4^- anion in the defect free $NaAlH_4$ lattice [26].

Acknowledgments

AA and PAG acknowledge the financial support from MIUR (PRIN 2007) and from the CARIPLO Foundation (Milan). DC wishes to thank the CNR and the "Firenze Hydrolab" project for support.

Appendix A.

A.1. Data reduction

Spectra were grouped into two distinct data blocks (*i.e.* forward-scattering and backscattering data, respectively). This grouping procedure is justified by the narrow angular range spanned by the detectors of each block, since the corresponding full-width-at-half-maximum, $\Delta\theta$, was estimated to be only 8° [13]. In this way, we produced double-differential cross-section measurements along the TOSCA-II kinematic paths Q=$Q_{F,B}(E)$ (for forward-scattering and backscattering spectra, respectively) of each sample-plus-can system, plus the empty can. Data were then corrected for the $(E_1/E_0)^{1/2}$ kinematic factor, and the empty-can contribution was properly subtracted [27] taking into account the E_0-dependent sample transmission.

A.2. Data analysis details

A.2.1. Thermally untreated samples

Standard corrections for self-absorption attenuation and multiple scattering contamination were carried out, even though samples #1 and #3 have a quite large transmission (T = 94.3% and 95.8% at E_0 = 100 meV, respectively) and hence a modest scattering power. These procedures were performed through the analytical approach suggested by Agrawal and by Sears in the case of a flat slab-like geometry [28]. This method needed two important inputs, which are related to the microscopic dynamics of the measured sample, namely: (a) the total scattering cross-section of the sodium aluminohydrides, $\sigma_t(E_0)$, known to be largely dependent on E_0 because of H; (b) an estimate of the sample scattering law to be folded with itself in order to generate multiple scattering contributions. Both procedures (*i.e.* self absorption and multiple scattering corrections) were accomplished in the framework of the incoherent approximation [29], justified by the preponderance of the proton scattering and by the polycrystalline nature of the samples.

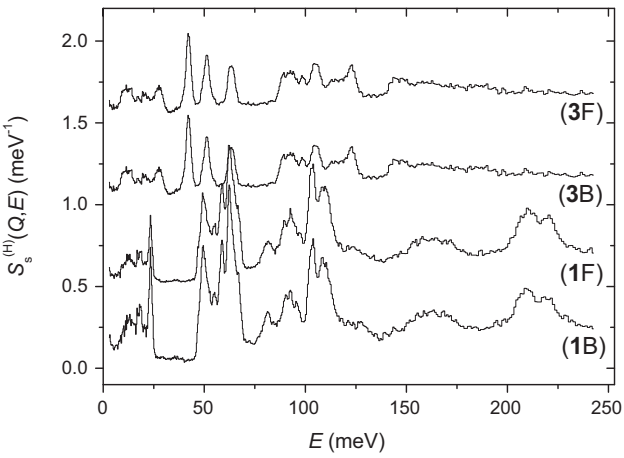

Fig. A1. Hydrogen component of the self inelastic structure factor from the Ti-doped thermally untreated $NaAlH_4$ and Na_3AlH_6 samples (#1 and #3, cf. Table 1), recorded in backscattering (B) and forward scattering (F) at T = 16 K. Spectra have been vertically shifted.

The sample total scattering cross-section, $\sigma_t(E_0)$, was estimated adding the small metal contribution (*i.e.* bound cross-section, constant in E_0) to the large, E_0-dependent, H part. Multiple scattering contributions were found to be quite modest, but not entirely negligible, in the energy transfer interval 3–250 meV, containing the single-phonon scattering. These contributions were carefully evaluated and finally subtracted, together with the (simulated) small metal signal. The resulting spectra are reported in Fig. A1 as incoherent inelastic protons (H-atoms) structure factor, $S_s^{(H)}(Q, E)$, for samples #1 and #3.

A.2.2. Thermally treated samples

Samples #2 and #4 were treated as homogeneous mixtures of $NaAlH_4$, Na_3AlH_6 and NaH in order to correct for self-absorption attenuation and multiple scattering contaminations. The concentrations of these three species in the two samples were estimated, approximately, via a simple fit on raw data making use of a linear combination of the uncorrected spectra 1 and 3 plus the equivalent low-temperature measurement on NaH [24]. The following molar compositions were found: for 2: [$NaAlH_4$] = 30%, [Na_3AlH_6] for 4: [Na_3AlH_6] = 85%, [NaH] = 15%. These values were employed for the data reduction as in the previous subsection, yielding the following average estimates of the *generalized self inelastic structure*:

$$\Sigma_s(Q, E) = \sum_n x_n \sigma_n S_s^{(n)}(Q, E), \tag{A1}$$

where x_n is the molar concentration of the nth species, σ_n is the total scattering cross-section of the nth species, and the sum over n is running on all the non-equivalent atomic species. These neutron spectra are shown in Fig. A2. The fitting procedure making use of $\Sigma_s(Q,E)$ yielded an excellent spectral reconstruction for both thermally activated samples and more accurate compositions: $[NaAlH_4]_{\#2}$ = 31.3(9)%, $[Na_3AlH_6]_{\#2}$ = 68.7(9)%, $[NaH]_{\#2}$ = 0.0(9)%, and $[NaAlH_4]_{\#4}$ = 0.0(6)%, $[Na_3AlH_6]_{\#4}$ = 86.7(6)%, and $[NaH]_{\#4}$ = 13.3(6)%.

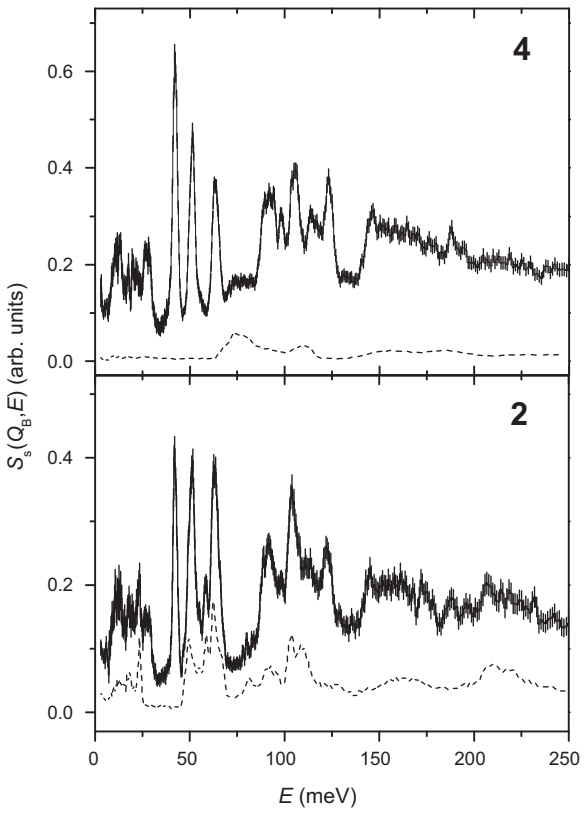

Fig. A2. Generalized self inelastic structure factor from the Ti-doped thermally treated $NaAlH_4$ and Na_3AlH_6 samples (#2 and #4, cf. Table 1), recorded in backscattering at $T = 16$ K. In addition, $NaAlH_4$ and NaH contributions to the thermally activated spectra (*i.e.* to #2 and #4, respectively) have been also added as dashed lines. Spectra have been vertically shifted for graphic reasons.

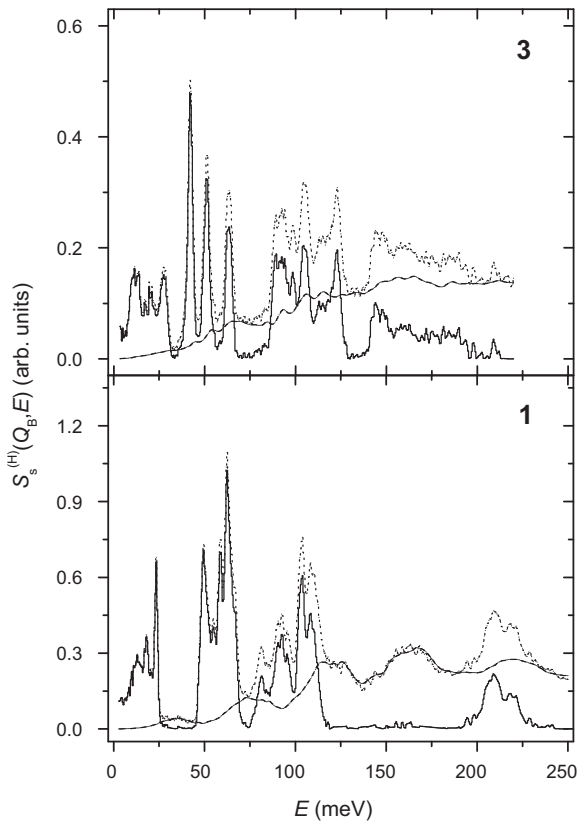

Fig. A3. Total (dotted lines), one-phonon (full lines), and multiphonon (dashed lines) terms of the hydrogen self inelastic structure factors from Ti-doped $NaAlH_4$ (#1) and Na_3AlH_6 (#3) samples measured in backscattering (see Table 1). The two total terms in panels 1 and 3 are equivalent to plots 1 and 3 in Fig. 2 of the main text, respectively.

A.3. Calculation of the phonon contribution.

The one-phonon proton component in the spectra, $S^{(H)}_{s,+1}(Q,E)$, can be obtained [28] from the following equation:

$$S^{(H)}_{s,+1}(Q,E) = \left\langle \exp[-2W_H(\mathbf{Q})] \sum_q \sum_{j=1}^{r} \frac{\hbar \left| \mathbf{Q} \cdot \boldsymbol{\sigma}^{(H)}_j(\mathbf{q}) \right|^2}{2M_H \omega_j(\mathbf{q})} \times [1 + n_j(\mathbf{q})] \delta[E - \hbar\omega_j(\mathbf{q})] \right\rangle, \quad \text{(A2)}$$

where $\exp[-2W_H(\mathbf{Q})]$ is the Debye–Waller factor for the hydrogen atom; r is the number of phonon branches labeled by j; while $\mathbf{q}$, $\omega_j(\mathbf{q})$, and $n_j(\mathbf{q})$ are the phonon wave-vector, frequency, and thermal population, respectively; $\boldsymbol{\sigma}^{(H)}_j(\mathbf{q})$ is the H polarization vector related to the phonon mode $(\mathbf{q}, j)$, M_H is the proton mass; and finally symbol $\langle \cdots \rangle$ stands for the powder average over the $\mathbf{Q}$ orientation. When dealing with Na_3AlH_6, however, a further average over the three non-equivalent types of protons also has to be assumed. The physical quantity reported in Eq. (A2) still retains a dependence on $Q(E)$ (*i.e.* on the spectrometer) through $2W_H(\mathbf{Q})$ and the squared modulus, but while the latter can be extracted by a trivial Q^2 product, the former remains rather complex considering the exact definition of $2W_H(\mathbf{Q})$ [30]. Approximating Eq. (A2) with:

$$S^{(H)}_{s,+1}(Q,E) \cong \frac{\hbar^2 Q^2}{2M_H E} \exp\left(-\frac{1}{3} Q^2 \langle \mathbf{u}^2_H \rangle\right) \times \left\langle \sum_q \sum_{j=1}^{r} |\hat{\mathbf{Q}} \cdot \sigma^{(H)}_j(\mathbf{q})|^2 \delta[E - \hbar\omega_j(\mathbf{q})] \right\rangle [1 + n(E)], \quad \text{(A3)}$$

after some algebraic manipulations, one finds:

$$S^{(H)}_{s,+1}(Q,E) \cong \frac{\hbar^2 Q^2}{2M_H E} \exp\left(-\frac{1}{3} Q^2 \langle \mathbf{u}^2_H \rangle\right) Z_H(E)[1 + n(E)] \quad \text{(A4)}$$

where $\langle \mathbf{u}^2_H \rangle$ is the mean squared displacement of the H atom and is related to the so-called "isotropic thermal factor" in diffraction, $B_{H,iso}$, through: $\langle \mathbf{u}^2_H \rangle = 3B_{H,iso}/8\pi^2$. To determine the multiphonon contributions in the TOSCA-II neutron spectra, we have used a self-consistent procedure [31] successfully applied in a number of cases [24]. Despite the approximations involved (*i.e.* a purely harmonic, isotropic and single-site treatment of the multiphonon terms), the results for both $NaAlH_4$ and Na_3AlH_6, see Fig. A3, show a satisfactory convergence of the procedure allowing a reliable extraction of the one-phonon component of the two spectra using the Eq. (A4). Relying on the internal self-consistent estimate of the H mean squared displacement and employing both backscattering and forward-scattering $S^{(H)}_{s,+1}(Q,E)$ data, one can assume $\langle \mathbf{u}^2_H \rangle = (0.072 \pm 0.005)\,\text{Å}^2$ and $(0.073 \pm 0.001)\,\text{Å}^2$, respectively for $NaAlH_4$ and Na_3AlH_6 (both at T=16 K).

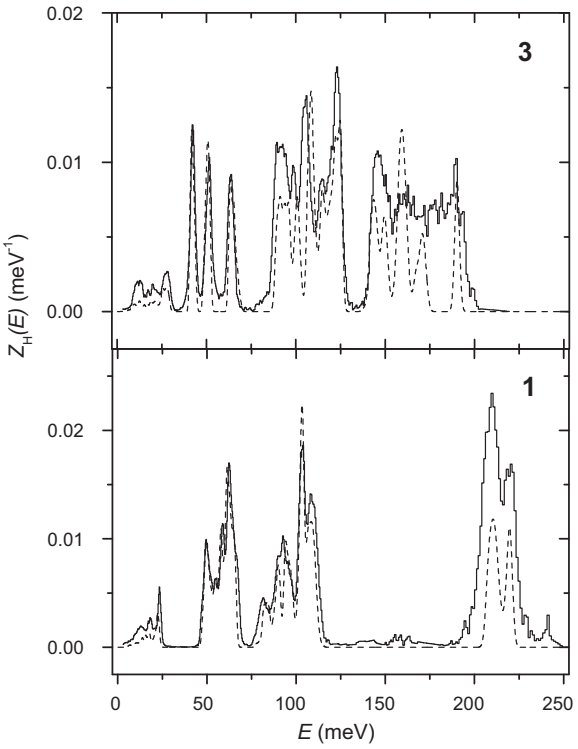

Fig. A4. Experimental hydrogen-projected density of phonon states from Ti-doped $NaAlH_4$ (panel 1, full line) and Na_3AlH_6 (panel 3, full line) samples. The simulated hydrogen-projected densities of phonon states (dashed line) are also shown.

Using these $\langle \mathbf{u}_H^2 \rangle$ values one can finally obtain the $Z_H(E)$, shown Fig. A4.

A.4. Calculation of the scattering section

The total scattering section, $\sigma_t(E_0)$ was calculated adding the metal contribution to the E_0 dependent H-scattering part. The latter was estimated from the simulated one-phonon neutron inelastic spectra, see below for $NaAlH_4$ (#1) and Na_3AlH_6 (#3), making use of Eqs. (3), (11) and (12) of Ref. [31]. A similar choice was made for the model self scattering laws, $S_S^{(n)}(Q, E)$, (n ≡ Na, Al, H) to be used for the multiple scattering estimate.

References

[1] F. Schüth, Nature 434 (2005) 712;
M.S. Dresselhaus, I.L. Thomas, Nature 414 (2001) 332.
[2] L. Schlapbach, A. Züttel, Nature 414 (2001) 353;
J. Yang, A. Sudik, C. Wolverton, D.J. Siegel, Chem. Soc. Rev. 39 (2010) 656;
J. Graetz, Chem. Soc. Rev. 38 (2009) 73.
[3] W.M. Mueller, J.P. Blackledge, G.G. Libowitz, Metal Hydrides, Academic Press, New York, 1968;
W. Grochala, P.P. Edwards, Chem. Rev. 107 (2007) p4152;
S. Orimo, Y. Nakamori, J.R. Eliseo, A. Züttel, C.M. Jensen, Chem. Rev. 107 (2007) 4111;
G. Walker (Ed.), Solid-state Hydrogen Storage, Woodhead Publ. Lim., Cambridge, 2010.
[4] G.E. Froudakis, J. Phys.: Condens. Matter 14 (2002) R453;
O.K. Alekseeva, L.N. Padurets, P.P. Parshin, A.L. Shilov, Russ. J. Inorg. Chem. 52 (2007) 34;
M.D. Ward, Science 300 (2003) 1104;
A.M. Seayad, D.M. Antonelli, Adv. Mater. (2004) 16;
G. Ferey, Chem. Soc. Rev. 37 (2008) 191;
S. Morike, S. Shimomura, S. Kitagawa, Nat. Chem. 1 (2009) 695.
[5] B. Bogdanović, M. Schwickardi, J. Alloys Compd. 253–254 (1997) 1.
[6] J. Graetz, J.J. Reilly, J.A. Johnson, Yu. Ignatov, T.A. Tyson, Appl. Phys. Lett. 85 (2004) 500.
[7] J. Íñiguez, T. Yildirim, Appl. Phys. Lett. 86 (2005) 103109.
[8] S. Chaudhuri, J.T. Muckerman, J. Phys. Chem. B 109 (2005) 6952.
[9] O. Palumbo, R. Cantelli, A. Paolone, C.M. Jensen, S.S. Srinivasan, J. Phys. Chem. B 109 (2005) 1168;
O. Palumbo, A. Paolone, R. Cantelli, C.M. Jensen, M. Sulić, J. Phys. Chem. B 110 (2006) 9105.
[10] P.C.H. Mitchell, S.F. Parker, A.J. Ramirez-Cuesta, J. Tomkinson, Vibrational Spectroscopy with Neutrons with applications in Chemistry, World Scientific, Singapore, 2005.
[11] J. Íñiguez, T. Yildirim, T.J. Udović, M. Sulić, C.J. Jensen, Phys. Rev. B 70 (2004) 060101.
[12] Q.J. Fu, A.J. Ramirez-Cuesta, S.C. Tsang, J. Phys. Chem. B 110 (2006) 711.
[13] D. Colognesi, M. Celli, F. Cilloco, R.J. Newport, S.F. Parker, V. Rossi-Albertini, F. Sacchetti, J. Tomkinson, M. Zoppi, Appl. Phys. A 74 (Suppl. 1) (2002) 64.
[14] R.A. Zidan, S. Takara, A. Hee, C.M. Jensen, J. Alloys Compd. 285 (1999) 119.
[15] J. Huot, S. Boily, V. Guther, R. Schultz, J. Alloys Compd. 283 (1999) 304.
[16] M.D. Segall, P.J.D. Lindan, M.J. Probert, C.J. Pickard, P.J. Hasnip, S.J. Clark, M.C. Payne, J. Phys.: Condens. Matter 14 (2002) 2717.
[17] S.J. Clark, M.D. Segall, C.J. Pickard, P.J. Hasnip, M.J. Probert, K. Refson, M.C. Payne, Z. Kristallogr. 220 (2005) 567.
[18] K. Refson, P.R. Tulip, S.J. Clark, Phys. Rev. B 73 (2006) 155114.
[19] J.P. Perdew, K. Burke, M. Ernzerhof, Phys. Rev. Lett. 77 (1996) 3865.
[20] P. Canton, M. Fichtner, C. Frommen, A. Leon, J. Phys. Chem. B 110 (2006) 3051;
E. Rönnebro, D. Noréus, K. Kadir, A. Reiser, B. Bogdanovic, J. Alloys Compd. 299 (2000) 101.
[21] X. Gonze, Phys. Rev. B 55 (1997) 10337.
[22] A.J. Ramirez-Cuesta, Comput. Phys. Commun. 157 (2004) 226.
[23] T.J. Udovic, D.A. Neumann, J. Leão, C.M. Brown, Nucl. Instrum. Methods A 517 (2004) 189.
[24] G. Auffermann, G.D. Barrera, D. Colognesi, G. Corradi, A.J. Ramirez-Cuesta, M. Zoppi, J. Phys.: Condens. Matter 16 (2004) 5731.
[25] T.M. Ivancic, S.-J. Hwang, R.C. Bowman Jr., D.S. Birkmire, C.M. Jensen, T.J. Udovic, M.S. Conradi, J. Phys. Chem. Lett. 1 (2010) 2412.
[26] F. Zhang, Y. Wang, M.Y. Chou, Faraday Discuss. 151 (2011) 243.
[27] H.H. Paalman, C.J. Pings, J. Appl. Phys. 33 (1962) 2635.
[28] A.K. Agrawal, Phys. Rev. A 4 (1971) 1560; V.F. Sears, Adv. Phys. 24 (1975) 1.
[29] M.M. Bredov, B.A. Kotov, N.M. Okuneva, V.S. Oskotskii, A.L. Shakh-Budagov, Sov. Phys. Solid State 9 (1967) 214.
[30] S.W. Lovesey, Theory of Neutron Scattering from Condensed Matter, Clarendon Press, Oxford, 1984.
[31] J. Dawidowski, J.R. Santisteban, J.R. Granada, Physica B 271 (1999) 212.